Chem

CellPress

Article

Carbon-centered radical capture at nickel(II) complexes: Spectroscopic evidence, rates, and selectivity

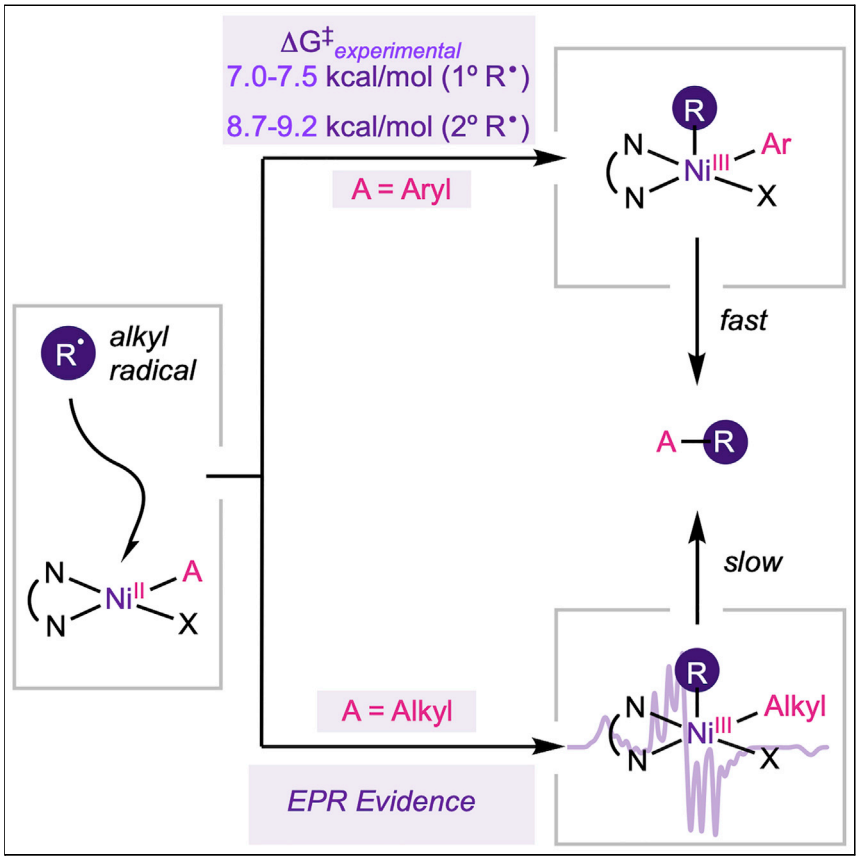

The capture of carbon-centered radicals at a nickel(II) center is commonly featured in recent cross-coupling and metallaphotoredox catalytic reactions. Despite its widespread application in catalysis, this fundamental step lacks experimental characterization. This report discloses the electron paramagnetic resonance (EPR) evidence for the formation of a nickel(III) intermediate, calibrates the capture rates to be on the scale of 10^7 and 10^6 $M^{-1}s^{-1}$ for primary and secondary radicals, respectively, and verifies the diastereoselectivity and enantioselectivity conferred by ligand effects.

Qiao Lin, Ethan H. Spielvogel, Tianning Diao

diao@nyu.edu

Highlights

Rates of radical capture by nickel(II) are on the scale of 10^6~10^7 $M^{-1}s^{-1}$

Nickel(III) intermediates derived from radical trapping are observed by EPR spectroscopy

There are different rate-determining steps for C(sp^3)–C(sp^3) and C(sp^3)–C(sp^2) bond formation

Stereoselectivity is conferred by radical capture with evident ligand control

Lin et al., Chem 9, 1–14
May 11, 2023 © 2023 Published by Elsevier Inc.
https://doi.org/10.1016/j.chempr.2023.02.010

Please cite this article in press as: Lin et al., Carbon-centered radical capture at nickel(II) complexes: Spectroscopic evidence, rates, and selectivity, Chem (2023), https://doi.org/10.1016/j.chempr.2023.02.010

Chem

CellPress

Article

Carbon-centered radical capture at nickel(II) complexes: Spectroscopic evidence, rates, and selectivity

Qiao Lin,[1] Ethan H. Spielvogel,[1] and Tianning Diao[1,2,*]

SUMMARY

The capture of carbon-centered radicals at a nickel(II) center is commonly featured in recent cross-coupling and metallaphotoredox catalytic reactions. Despite its widespread application in catalysis, this fundamental step lacks experimental characterization. This report portrays radical capture at catalytically relevant nickel(II) centers from several aspects, including the structure-activity relationships of the ligands, the mechanism, the kinetics, and the stereoselectivity. Spectroscopic data provide evidence for the formation of a nickel(III) intermediate. Strikingly different reactivity between nickel-aryl and nickel-alkyl complexes implies different rate-determining steps for C(sp^3)–C(sp^3) and C(sp^2)–C(sp^3) bond formation. Kinetic data benchmark the capture rates on the scale of 10^7 $M^{-1}s^{-1}$ and 10^6 $M^{-1}s^{-1}$ for primary and secondary radicals, respectively. Overall, the activation energy is higher than that of previous computational estimations. Finally, stoichiometric experiments with well-defined chiral nickel complexes demonstrate that the radical trapping step can confer diastereoselectivity and enantioselectivity with a drastic ligand effect.

INTRODUCTION

Recent advancements in cross-coupling reactions and metallaphotoredox catalysis exploit the reactivity of nickel catalysts to initiate and propagate radical reactions.[1–5] A commonly proposed intermediate step involved in these catalytic cycles features the capture of a carbon-centered radical at the nickel(II) center, generating a nickel(III) intermediate that can readily undergo reductive elimination (Figure 1A).[6] This pathway differs from traditional two-electron processes, frequently mediated by palladium and other noble metals, and provides novel synthetic opportunities for forming C–C bonds. For example, cross-coupling reactions catalyzed by nickel allow for stereo-convergent synthesis.[7] The ability of nickel to capture radical intermediates and engage them in cross-coupling reactions has broadened the scope of cross-coupling partners. Although radicals can be generated from halogen-atom abstraction by a low-valent nickel species,[8] abundant photoredox and electrocatalytic approaches have been developed for the formation of radicals from a wide range of precursors, including carboxylic acids, C–H bonds, boronates, and redox auxiliaries.[5,9–11] Moreover, the formation of a high-valent nickel(III) intermediate upon radical capture could promote C–C bond-forming reductive elimination both kinetically and thermodynamically.[12,13] Finally, the trapping of radicals at the nickel center can determine the chemoselectivity in cross-electrophile coupling reactions[14] and control stereoselectivity in diastereoselective and enantioselective coupling reactions.[15,16]

THE BIGGER PICTURE

First-row transition-metal complexes represent sustainable and affordable catalysts for organic synthesis. Because of their stable radical states, first-row metal catalysts can mediate radical pathways in catalysis by initiating radical formation via redox processes and capturing a radical at the metal center. Nickel(II) complexes are proposed to trap carbon radicals and engage in subsequent C–C bond formation from the nickel(III) intermediate. This fundamental step has broadened the scope of cross-coupling partners, enabled stereoconvergent synthesis, and controlled stereo- and chemoselectivity. Yet, there is a lack of experimental characterization of this critical step. This report provides spectroscopic evidence for radical capture, calibrates the rates, and demonstrates ligand-controlled stereoselectivity. These results help form hypotheses on reaction design with radical capture as an intermediate step and inform reaction optimization to achieve a broad scope.

Radical capture at a nickel complex formally increases its oxidation state by +1 and has been observed and characterized in several systems, including the transformations of Ni(I) to Ni(II),[17] Ni(II) to Ni(III),[18–20] and Ni(III) to Ni(IV).[20,21] The most catalytically relevant system is *N*-ligand coordinated Ni(II)-aryl complexes, such as (bpy)Ni(Ar)(Br) (bpy = bipyridine), which have been investigated computationally. Two possible pathways are generally considered: the first is an inner-sphere mechanism that involves the formation of a discrete Ni(III) intermediate, and the second is an outer-sphere mechanism in which C–C bonds are directly formed without an interaction between the entering radical and the nickel center (Figure 1B). The former has been proposed for primary and secondary radicals,[22–31] whereas the latter proved plausible for tertiary radicals.[24] Calculated kinetic barriers ($\Delta G^{\ddagger}$) vary among different studies (Figure 1C).[32] The capture of benzyl radical has been calculated to be almost barrierless,[22,25] whereas the activation energy for the slower secondary and tertiary radicals spreads across a range of values.[23,24,27] The estimated fast radical capture has precluded the consideration of this step as rate-limiting relative to the following reductive elimination in these computational studies. There is generally a lack of experimental characterization of radical capture at catalytically competent nickel(II) complexes to benchmark computational results, and previous studies seldom compared the effect of actor ligands on nickel radical capture.[31]

Herein, we address the knowledge gap with a comprehensive experimental study on radical capture at nickel(II)-aryl and nickel(II)-alkyl complexes bearing ligands commonly applied in catalytic reactions, such as bpy and phen (phen = 1,10-phenanthroline). The study sheds light on several key mechanistic aspects of radical capture at these nickel centers and reaches unforeseen conclusions: (1) experimental data distinguish inner-sphere and outer-sphere pathways and provide spectroscopic evidence for a nickel(III) intermediate; (2) experimental characterization of rate constants reveals that previous density functional theory (DFT) calculations generally underestimated the kinetic barrier and that radical capture at the nickel(II) could be rate limiting in relation to fast reductive elimination; (3) contrasting reactivity between nickel-aryl and alkyl complexes unveils different rate-determining steps, which accounts for synthetic challenges in forming C(sp^3)–C(sp^3) bonds and prompts reconsideration of the mechanism; and (4) investigations of the stereochemistry at the radical capture step elucidate the impact of the substrates and the chiral ligands on the stereochemical outcome. These results help form hypotheses on reaction design with radical capture as an intermediate step and inform reaction optimization to achieve a broad scope.

RESULTS AND DISCUSSION

Effect of actor and auxiliary ligands on nickel

We conducted a survey of various phen-, pyrox-, pybox-, and bpy-nickel complexes to establish the effects of the auxiliary and actor ligands on radical capture. Benzyl dihydropyridine **1** (Bn–DHP) has been shown to eject benzyl radical upon photoexcitation, driven by the formation of the resulting Hantzsch pyridine.[33] When we irradiated **1** with 390 nm light in the presence of (phen)Ni(Ar)(Br) complex **2**, we observed the formation of the cross-coupling product Ar-Bn in quantitative yields (Figure 2A, entry 1). Monitoring the reaction with UV-visible spectroscopy and comparing the spectra with that of (phen)NiBr **3** verified the concomitant formation of (phen)NiBr **3** (Figure S6). Control experiments revealed that **2** is stable under photo-irradiation and ruled out possible transformations of **2** induced by direct photoexcitation.[34] The yield of the cross-coupling product was substantially

[1]Department of Chemistry, New York University, 100 Washington Square East, New York, NY 10003, USA

[2]Lead contact

*Correspondence: diao@nyu.edu

https://doi.org/10.1016/j.chempr.2023.02.010

Please cite this article in press as: Lin et al., Carbon-centered radical capture at nickel(II) complexes: Spectroscopic evidence, rates, and selectivity, Chem (2023), https://doi.org/10.1016/j.chempr.2023.02.010

CellPress

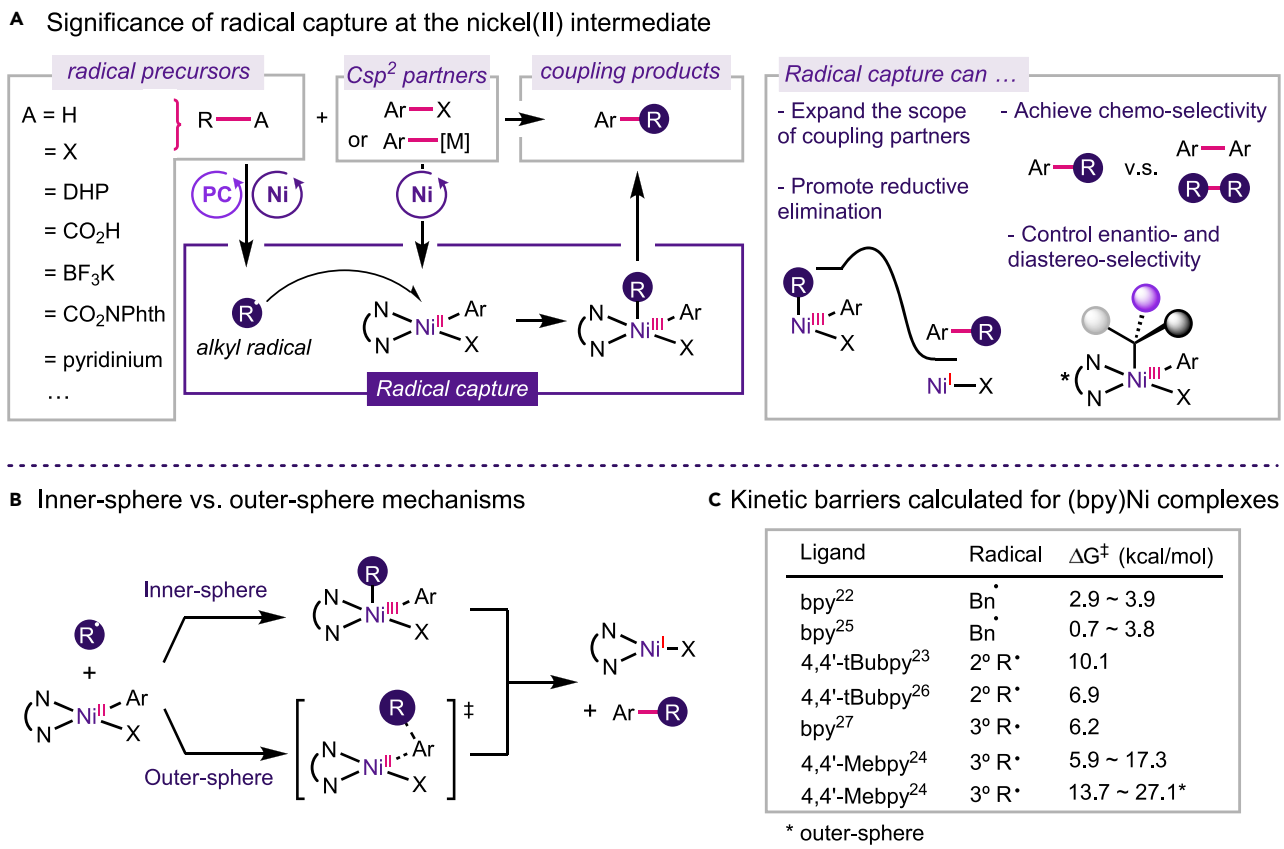

Figure 1. Radical capture at the nickel(II) center as a key step in nickel-catalyzed cross-coupling and metallaphotoredox catalytic reactions

reduced to 10% with the bulky complex **4** (entry 2). Ni-alkyl complexes **5** and **6** lacked reactivity and generated cross-coupling and homo-coupling products in low yields (entries 3 and 4).[35] The fate of the benzyl radical in these cases was toluene, whereas the remaining nickel complexes and **1** stayed intact. Complex **7** afforded biaryl coupling as the major product, consistent with previous reports of the complexes' instability (entry 5).[36]

We then examined nickel complexes bearing different *N*-ligands, including bpy, $^{t\mathrm{Bu}}$bpy ($^{t\mathrm{Bu}}$bpy = di-*tert*-butyl-bipyridine), $^{\mathrm{CF3}}$bpy ($^{\mathrm{CF3}}$bpy = di-trifluoromethyl-bipyridine), pyrox (pyrox = pyridine-oxazoline), and pybox (pybox = pyridine-bis-oxazoline)[7] (Figure 2A, entries 6–12). Good yields of the C(sp^2)–C(sp^3) cross-coupling products were observed across a range of ligand classes. $^{t\mathrm{Bu}}$bpy is more commonly applied in catalysis than bpy, primarily for better solubilization of nickel complexes in organic solvents. Both $^{t\mathrm{Bu}}$bpy and bpy gave similar yields of the cross-coupling product (entries 6 and 7). The electron-deficient complex **10** (entry 8) led to a slightly lower yield than **8** and **9**. The yield of cross-coupling product formed from ($^{i\mathrm{Pr}}$pybox)Ni complex **14** was noticeably lower than the yield of those formed with bidentate ligands. We attribute this decrease in reactivity to the steric bulk of the isopropyl groups on pybox. When subjected to reaction conditions in Figure 2A, the corresponding bpy and pyrox-ligated nickel-alkyl complexes only yielded trace amounts of the C(sp^3)–C(sp^3) cross-coupling products (entries 9 and 11). This trend is consistent with the hybridization effect observed for the (phen)Ni analogs: (phen)Ni-aryl complexes are efficient in mediating C(sp^2)–C(sp^3) bond formation after accepting

Please cite this article in press as: Lin et al., Carbon-centered radical capture at nickel(II) complexes: Spectroscopic evidence, rates, and selectivity, Chem (2023), https://doi.org/10.1016/j.chempr.2023.02.010

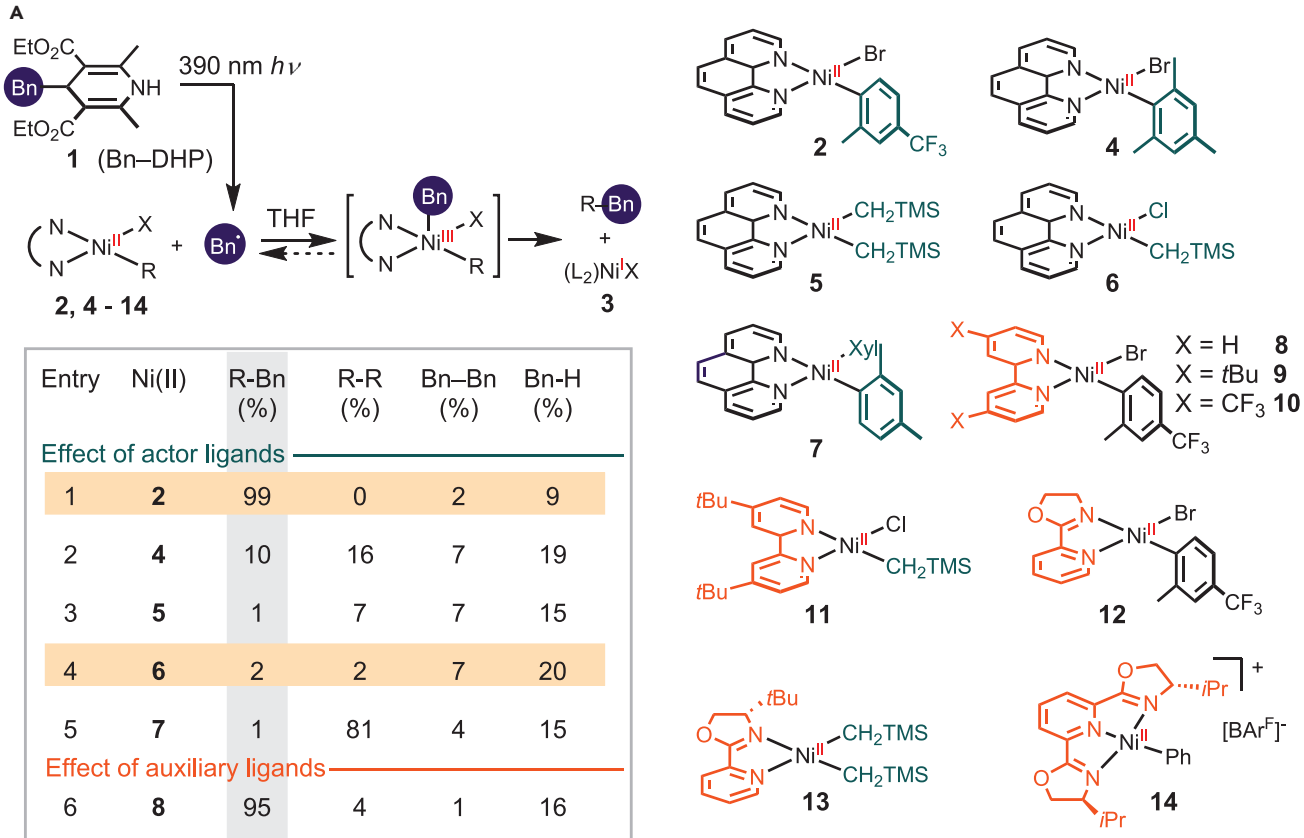

Entry	Ni(II)	R-Bn (%)	R-R (%)	Bn–Bn (%)	Bn-H (%)
Effect of actor ligands					
1	**2**	99	0	2	9
2	**4**	10	16	7	19
3	**5**	1	7	7	15
4	**6**	2	2	7	20
5	**7**	1	81	4	15
Effect of auxiliary ligands					
6	**8**	95	4	1	16
7	**9**	92	3	4	18
8	**10**	81	8	3	20
9	**11**	1	2	7	18
10	**12**	90	2	10	14
11	**13**	1	13	9	23
12	**14**	75	0	17	11

[a]GC yields.

Figure 2. Nickel(II)-mediated radical capture and C–C bond formation
Stoichiometrically (A) and catalytically (B).

the benzyl radical, but (phen)Ni-alkyl complexes gave little C(sp^3)–C(sp^3) cross-coupling products.

Different catalytic reactivity between C(sp^2) and C(sp^3) electrophiles

The strikingly different reactivity between **2** and **6** prompted us to probe the different catalytic reactivity between C(sp^2) and C(sp^3) electrophiles. We carried out catalytic reactions between DHP substrate **15** and bromide electrophiles under the conditions reported by Melchiorre and co-workers (Figure 2B, equation 1).[33] Although aryl bromide underwent smooth conversion to the cross-coupling product **16**, consistent with the report,[33] *n*-propyl bromide led to no C(sp^3)–C(sp^3) coupling products **17**.

Please cite this article in press as: Lin et al., Carbon-centered radical capture at nickel(II) complexes: Spectroscopic evidence, rates, and selectivity, Chem (2023), https://doi.org/10.1016/j.chempr.2023.02.010

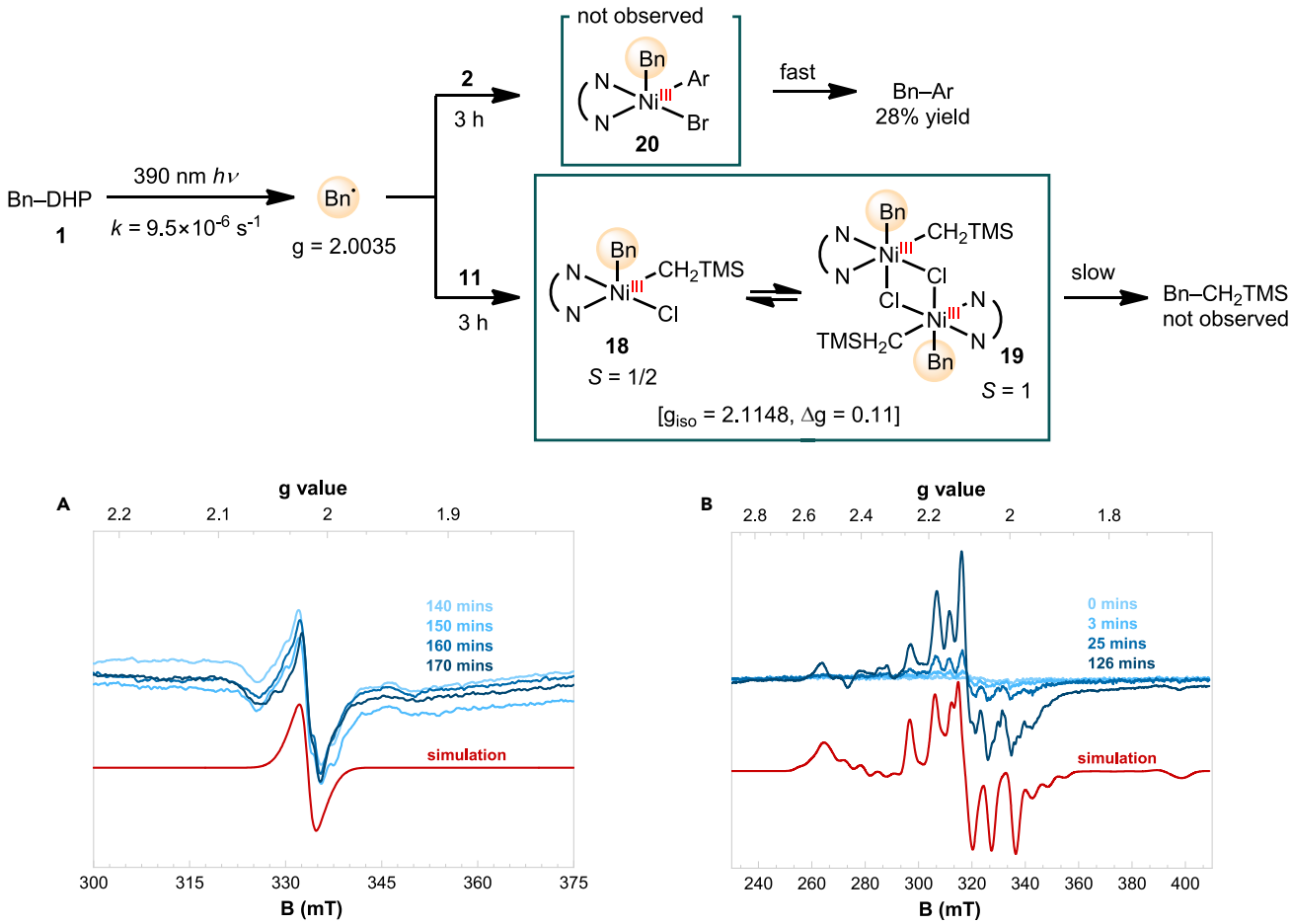

Figure 3. EPR study of radical capture by 2 and 11

Radical capture by (A) **2** at 77 K and (B) **11** at 5 K in THF under light irradiation (390 nm). [**1**] = 50 mM; [**2**] or [**11**] = 10 mM. The spectral data were collected with the following spectrometer settings: microwave power = 0.5 mW, modulation frequency = 100 KHz, modulation amplitude = (A) 10 G and (B) 4 G. The simulated spectra used the following parameters: (A) g = 2.0038; (B) a mixture of two species, **18** and **19** (**18**: S = 1/2, g = [2.2201, 2.1105, 2.0139], $A_{H,H}$ = [95, 10, 90; 0, 25, 0] G; **19**: S = 1, g = [2.2205, 2.1350, 2.0135], D = 0.061 cm^{-1}, $A_{N,N}$ = [40, 60, 0; 40, 60, 0] G).

Spectroscopic evidence for the formation of a nickel(III) intermediate upon capture

Subsequently, we performed photo-electron paramagnetic resonance (EPR) experiments to verify the formation of the Ni(III) species resulting from radical capture by phen and (^{tBu}bpy)Ni(II) complexes. Irradiation of Bn-DHP without any nickel species present afforded benzyl radical with a g_{iso} value of 2.0035 (Figure S7).[33] The rate of this photo-excited radical generation was determined to be slow ($k = 9.5 \times 10^{-6}\ s^{-1}$) (Figure S5). We then gathered EPR spectra of **1** in the presence of nickel complexes **2**, **9**, and **11** under 390 nm irradiation.[37] With **2** and **9**, we observed the accumulation of an isotropic signal at 77 K, which was assigned to benzyl radical, evident by the g_{iso} value of 2.0038 (Figures 3A and S10). The EPR spectrum displayed no signal corresponding to a nickel species. After irradiation for three hours, analysis of the reaction mixture of **2** by GC revealed the formation of the cross-coupling product in 28% yield. The rest of **1** and **2** remained unreacted.

Conducting the photo-EPR experiment on complex **11** resulted in the observation of no signal at 77 K but a metal-centered EPR signal at 5 K (Figure 3B), suggesting fast

temperature-dependent relaxation.[38] The signal, spanning between 240 and 400 mT, exhibited g_z turning points at g = 2.52 and g = 1.67, which correspond to the transition from m = +1 and m = −1 to m = 0 in the z direction, respectively.[39] This signal range is broader than that of a common S = 1/2 Ni(III) complex, usually between 300 and 340 mT.[40] The fast temperature-dependent relaxation and the multiple line shapes suggest a S = 1 species, the zero-field splitting (ZFS) of which accounts for the observed g_z turning points. We could thus calculate the magnitude of the D tensor to be 0.061 cm^{-1},[41] a ZFS parameter that implies a strong dipolar-dipolar interaction and a short distance between the two spins.[42] Simulation of the spectrum resulted in a mixture of a S = 1/2 and S =1 species with similar g values of [2.2201, 2.1105, 2.0139] and [2.2205, 2.1350, 2.0135], respectively (Figure S9). The resemblance of the g values to those reported for Ni(III) complexes prompted us to assign this signal to the monomeric and dimeric nickel(III) species, **18** and **19**.[12,13,42,43] The isotropic g_{iso} of 2.1148 and the small Δg = 0.11 falls into the range of expected values for nickel(III) complexes. DFT calculations performed with the ORCA package revealed that both **18** and the putative Ni(III) **20** are nickel-centered radicals (Figure S11).

Kinetics of radical capture by nickel(II) complexes

Direct kinetic measurements of the radical capture step were complicated by the slow generation of the benzyl radical and the fast reductive elimination from the (phen) and (^{tBu}bpy)Ni(III)-aryl intermediates. To circumvent this, we employed radical clock methods to determine rate constants for the radical capture at complexes **2** and **9**. The reduction of primary bromide **21** by Bu_3SnH under irradiation (365 nm) gave **23** and **25**. A seven-membered product from 7-*endo* cyclization of **27** was also observed in small quantity (Scheme S1). The reaction proceeds through the generation of $Bu_3Sn^{\bullet}$ upon irradiation of Bu_3SnH, which abstracts the bromine atom from **21** to generate **27**. Hydrogen-atom transfer (HAT) from Bu_3SnH to radical **27** (k_1) accounts for the formation of **23**. Competing with this pathway, 6-*exo* cyclization of **27** (k_2) is followed by HAT of **29** to generate **25**. The conversion of **27** to **23** is a bimolecular process depending on [Bu_3SnH], whereas 6-*exo* cyclization of **27** is unimolecular. Thus, the ratio of [**23**]/[**25**] is expected to display a linear dependence on [Bu_3SnH], under the assumption that radical cyclization to afford **29** and the subsequent HAT to form **25** are irreversible. We conducted parallel reactions by varying the concentrations of Bu_3SnH and recorded the ratios of [**23**]/[**25**] for each reaction at 10% conversion, when the consumption of Bu_3SnH was negligible relative to the large excess of initial [Bu_3SnH] (Figure 4A). The ratios of [**23**]/[**25**] displayed a linear relationship on [Bu_3SnH], the slope of which corresponds to the ratio of k_1/k_2. Given that k_1 was reported to be $(2.7 \pm 0.1) \times 10^6$ $M^{-1}s^{-1}$,[44] we solved for the unimolecular rate constant of 6-*exo* cyclization to be $k_2 = (2.8 \pm 0.1) \times 10^5$ s^{-1} (Figure 4A).

The rate of HAT for secondary radical **28** with Bu_3SnH has been reported to be $k_3 = (1.5 \pm 0.1) \times 10^6$ $M^{-1}s^{-1}$.[44] Applying the same method as described above for the analogous secondary bromide substrate, we measured 6-*exo* cyclization rate of secondary radical **28** to be $k_4 = (3.8 \pm 0.3) \times 10^5$ s^{-1} (Figure 4A). The rates of HAT for primary (k_1) and secondary (k_3) radicals are comparable, which reflects a minimal steric effect on cyclization. The cyclization rates of primary and secondary radicals, k_2 and k_4, are similar because the activation energy for radical cyclization is governed by the reorganization of the molecule to the proper geometry for cyclization rather than by sterics.[45,46]

The cyclization rate constants k_2 and k_4 for radicals **27** and **28** equipped us to determine the capture rates of **27** and **28** at nickel(II) complex **2**

Please cite this article in press as: Lin et al., Carbon-centered radical capture at nickel(II) complexes: Spectroscopic evidence, rates, and selectivity, Chem (2023), https://doi.org/10.1016/j.chempr.2023.02.010

CellPress

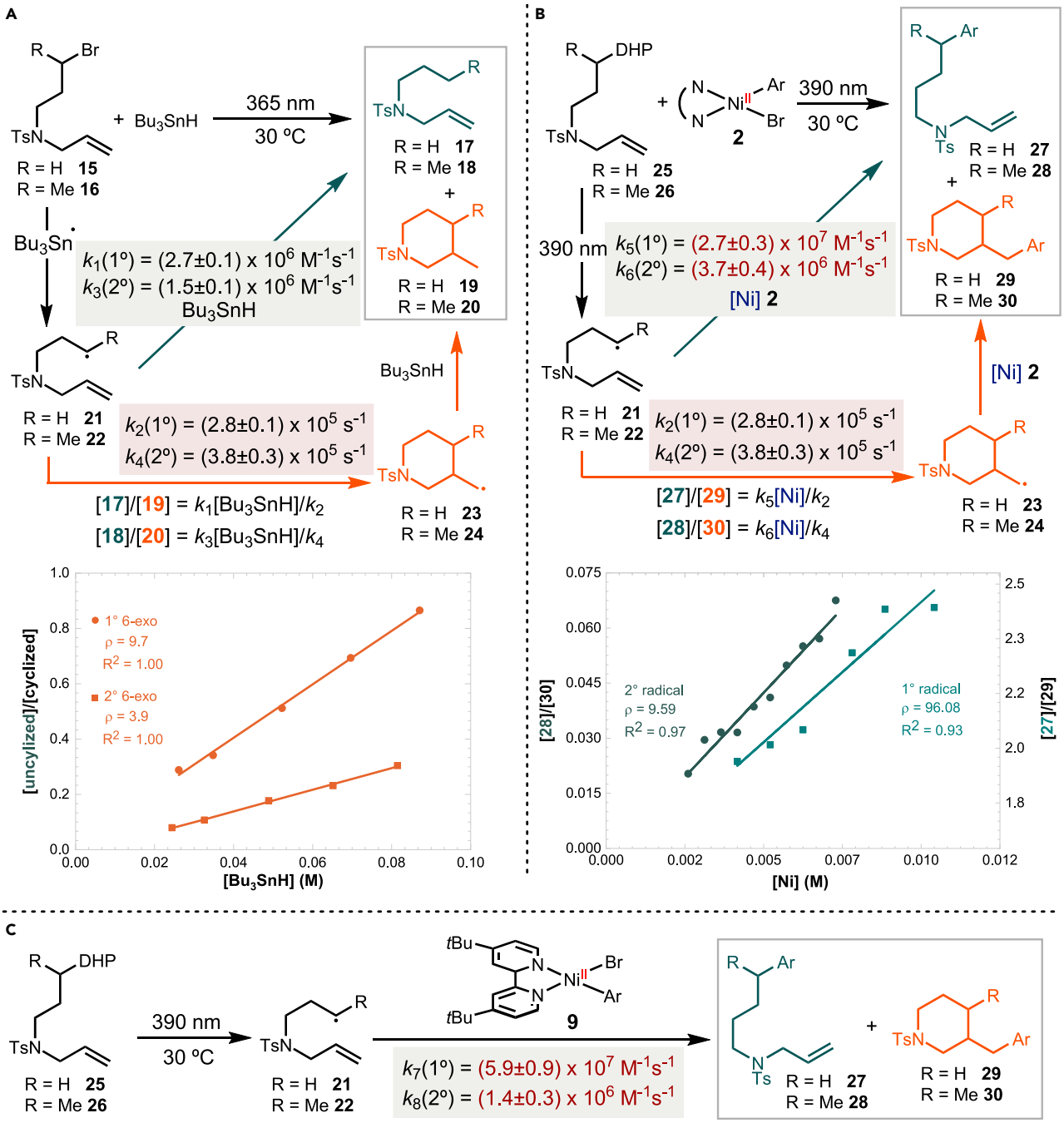

Figure 4. Determination of the primary and secondary radical capture rate with radical clock substrates

(A) Calibration of primary and secondary radical cyclization rates k_2 and k_4.

(B) Determination of the rates of primary and secondary radical capture at nickel(II) **2** k_5 and k_6.

(C) Determination of the rates of radical capture at nickel(II) **9** k_7 and k_8.

(Figure 4B). The DHP analog **31** was readily activated under 390 nm irradiation to generate **27**; this was followed by trapping by **2** and reductive elimination to afford cross-coupling products **33** and **35** (Figure 4B).[47] Analogous to the reduction of **21** by Bu_3SnH, the ratio of [**33**]/[**35**] is proportional to [**2**], and the slope of the linear fitting reflects the ratio of the rate constants of the competing pathways.

By varying [2], we determined the rate constant for the trapping of the primary radical **27** at (phen)Ni(Ar)(Br) to be k_5 = (2.7 ± 0.3) × 10^7 $M^{-1}s^{-1}$, which corresponds to a kinetic barrier $\Delta G^{\ddagger}$ of 7.5 kcal/mol at 30°C. Analyzing the product distribution of radical clock **32** under irradiation and in the presence of nickel(II) **2** revealed the second-order rate constant for radical capture of **28** by **2** to be k_6 = (3.7 ± 0.4) × 10^6 $M^{-1}s^{-1}$ ($\Delta G^{\ddagger}$ = 8.7 kcal/mol at 30°C), which is nearly an order of magnitude slower than that of the primary radical capture rate k_5 (Figure 4B).

Another commonly applied ligand in nickel catalysis is di-*tert*-butyl-bipyridine. Replacing complex **2** with complex **9** in this study revealed the rates of primary and secondary radical capture by **9** to be k_7 = (5.9 ± 0.9) × 10^7 $M^{-1}s^{-1}$ ($\Delta G^{\ddagger}$ = 7.0 kcal/mol at 30°C) and k_8 = (1.4 ± 0.3) × 10^7 $M^{-1}s^{-1}$ ($\Delta G^{\ddagger}$ = 9.2 kcal/mol at 30°C) (Figure 4C). Compared with k_7 and k_6, the higher rate of primary radical capture could be attributed to the lower oxidation potential of **9**, whereas the lower rate of secondary radical capture could result from the steric hindrance of the *tert*-butyl group on the bpy ligand.

An inner-sphere mechanism and rationale for the contrasting reactivity between Ni-C(sp^2) and Ni-C(sp^3) complexes

Collectively, the structure-activity relationship of ligands and the entering radical (Figure 2A), in combination with the EPR data (Figure 3), provide an experimental basis for distinguishing between inner- and outer-sphere mechanisms for radical capture at the nickel(II) center. The more hindered nickel center undergoes slower radical capture (Figure 2A, entry 2). This significant steric effect lends the initial support for an inner-sphere pathway. The formation of a nickel(III) intermediate would be hindered by the methyl groups of **4** oriented toward nickel in an inner-sphere mechanism, whereas such a steric effect would be insignificant if the benzyl radical approaches the aryl group in an outer-sphere pathway. The EPR signal of Ni(III) species **18** and **19** provides unambiguous evidence for radical capture at the (^{tBu}bpy)nickel(II)-alkyl center. The inner-sphere mechanism is consistent with previous DFT studies.[22–24] Nevertheless, the lack of a Ni(III) signal with complex **2** suggests that an outer-sphere mechanism cannot be fully ruled out at this point for nickel-aryl complexes.

Radical clock experiments elucidated the kinetic barriers for radical trapping at complexes **2** and **9** to be 7.5 and 7.0 kcal/mol for the primary radical and 8.7 and 9.2 kcal/mol for the secondary radical, respectively (Figure 4). The primary radical capture rates of (2.7 ± 0.3) and (5.9 ± 0.9) × 10^7 $M^{-1}s^{-1}$ are slower than the diffusion controlled bimolecular reaction rate of 2 × 10^{10} $M^{-1}s^{-1}$ (25°C)[44] and comparable to that measured for a macrocyclic nickel(I) complex (6 × 10^7 $M^{-1}s^{-1}$).[17] The barriers for primary radicals are noticeably higher than previous computational results.[22,25] The activation energy for secondary radicals is in line with some DFT results,[23,28] whereas it is higher than the others.[26,29,30] Admittedly, different ligands could vary the rates, as evident by the higher k_7 than k_5. The higher experimental activation energy compared with the computational data suggests that there is generally an underestimation of the activation energy for radical reactions, possibly because of the common limitation of current DFT methods.[48] The nearly 10-fold decrease in the rate with the secondary radical (k_6) relative to the primary radical (k_5) indicates that a bulkier entering radical could hinder radical capture.

The most striking result is the difference in reactivity between nickel-C(sp^2) complex **2** and nickel-C(sp^3) complex **6** (Figure 2A, entries 1 and 4). We considered two hypotheses to account for the lack of cross-coupling reactivity of **6**. In the first

Please cite this article in press as: Lin et al., Carbon-centered radical capture at nickel(II) complexes: Spectroscopic evidence, rates, and selectivity, Chem (2023), https://doi.org/10.1016/j.chempr.2023.02.010

CellPress

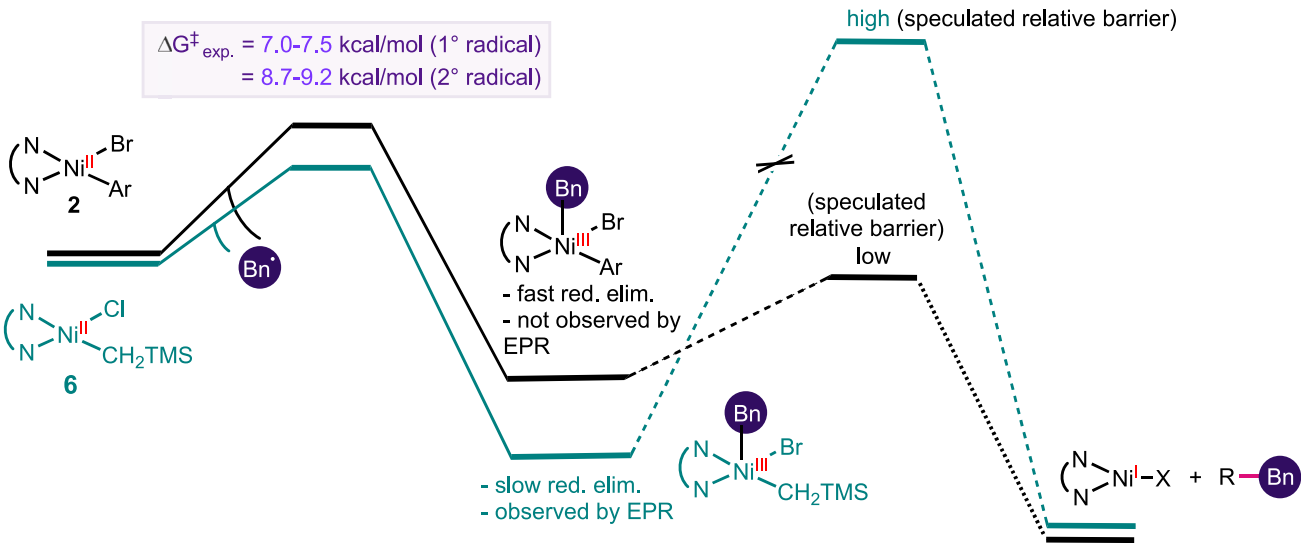

Figure 5. Proposed energy profile based on experimental findings that accounts for the different reactivity between nickel-aryl and alkyl complexes

scenario, radical capture was favorable at **2** but unfavorable at **6**. In the second scenario, both **2** and **6** could trap the radical, but reductive elimination from the nickel(III) intermediate was slower in forming C(sp^3)–C(sp^3) bonds relative to C(sp^2)–C(sp^3) bonds. The observation of nickel(III) species **18** and **19** by EPR spectroscopy (Figure 3B) suggests that a nickel-alkyl species, such as **6** and **11**, can readily trap benzyl radical, and the resulting nickel(III) intermediate might be stabilized by aggregating into a dimeric structure. Nickel(III) **18** and **19** afforded no reductive elimination product, which is consistent with the latter hypothesis that C(sp^3)–C(sp^3) bond-forming reductive elimination is difficult. In sharp contrast, complex **2** generated no nickel(III) signal that could be detected by EPR spectrometer, but efficiently furnished the cross-coupling product. The lack of a nickel-centered EPR signal suggests that the steady-state concentration of nickel(III) species from **2** is lower than the detection limit of 0.07 mM of the SHQE resonator. The low steady-state concentration of nickel(III) is consistent with fast reductive elimination to form C(sp^2)–C(sp^3) bonds. The energy profile for these pathways is summarized in Figure 5. Such a scenario was not widely considered in the previous computational results.

Rates of reductive elimination from the nickel(III) center follow the trend previously established in palladium and platinum-mediated C–C bond formation: C(sp^2)–C(sp^2) > C(sp^2)–C(sp^3) > C(sp^3)–C(sp^3).[49,50] A similar trend was also observed with well-defined nickel(III) complexes,[12,13] in DFT calculations,[31] and in the study of nickel(II) complexes.[51] Fast reductive elimination of nickel-aryl complexes could be attributed to the participation of the aryl π-orbitals that are in the proper orientation for forming new C–C bonds. In contrast, the σ-orbitals in a nickel-alkyl molecule requires reorientation to form new C–C bonds. A related but different phenomenon was observed when the reductive elimination rates of M(H)$_2$, M(H)(Me), and M(Me)$_2$ complexes were compared.[52] The relative stability of nickel(III) intermediates could also contribute to their different reactivity in reductive elimination. Alkyl groups are stronger σ-donors than aryl groups and can thus better stabilize the nickel(III)-alkyl species.

The different reactivity between **2** and **6** is aligned with the catalytical reactivity (Figure 2B, equation 1). Although aryl bromides proceeded to afford the cross-coupling

Please cite this article in press as: Lin et al., Carbon-centered radical capture at nickel(II) complexes: Spectroscopic evidence, rates, and selectivity, Chem (2023), https://doi.org/10.1016/j.chempr.2023.02.010

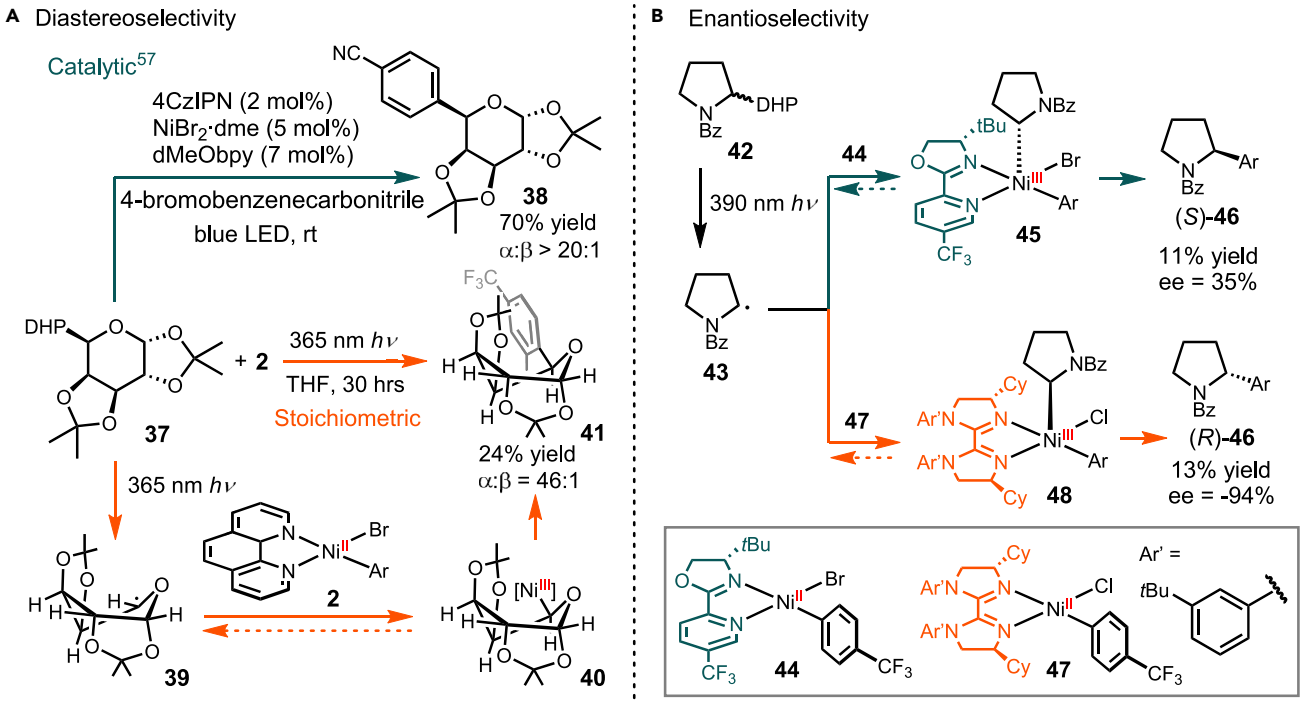

Figure 6. Radical capture at the nickel(II) center
Diastereoselectively (A) and enantioselectively (B).

product **16**, alkyl bromide did not generate the target product **17**. Nevertheless, facile C(sp^3)–C(sp^3) bond formation has been observed both catalytically[2,53–55] and stoichiometrically under optimized conditions.[56] Although the reactivity is subject to various ligand effects, the low reactivity of C(sp^3)–C(sp^3) bond-forming reductive elimination that was observed in this study implies that previous proposals for catalytic reactions might necessitate reconsideration, and our ongoing research seeks to resolve this question.

Diastereoselectivity and enantioselectivity

An eminent accomplishment of nickel-catalyzed cross-coupling reactions is the control of diastereoselectivity and enantioselectivity.[15,16] Although different stereo-determining steps could be proposed for various reactions, the observation of stereoselectivity from well-defined organonickel intermediates is critical for identifying factors that contribute to the stereoselectivity.[7] There have been limited examples of organometallic studies on the diastereo- and enantioselectivity of the radical capture step mediated by well-defined nickel intermediates.

Nickel-catalyzed diastereoselective coupling has been applied to a series of *C*-glycosylation reactions, which leverage the formation of glycosyl radicals that can then be added to nickel(II) intermediates and proceed to cross-coupling with high diastereoselectivity.[57–59] For example, photoredox coupling of glycosyl DHP **37** with 4-bromobenzenecarbonitrile furnished the α-glycosyl arene product **38** in high yield with an excellent diastereomeric ratio (d.r.) (Figure 6A).[57] To probe whether diastereoselectivity could be attained from the addition of glycosyl radical to nickel(II) intermediates, we performed the stoichiometric experiments and observed the resulting product distribution (Figure 6B). Irradiation of **37** in the presence of 1 equiv of **2** afforded glycosyl arene product **41** in 24% yield with a d.r. of

46:1. The low conversion is attributed to the slow activation of **37** in the absence of a photocatalyst.

Two mechanistic scenarios could be considered to account for the high diastereoselectivity. If the capture of **39** by **2** were irreversible, the high d.r. could be attributed to the preference of **2** to approach from the α-face of **39**. If reversible, the reaction would be under Curtin-Hammett control, where the d.r. would be dictated by faster reductive elimination of the α-glycosyl nickel intermediate **40** relative to the β-anomer. Studies to distinguish these two scenarios are underway. Nevertheless, the diastereoselectivity in the isolated step of glycosyl radical capture at the nickel center is comparable to catalytic reactions, indicating that radical capture could be the diastereoselective determining step and should be considered in future reaction design.

Radical capture at a chiral nickel complex has been exploited in enantioselective cross-coupling reactions.[15,16] In light of recent advancements in the asymmetric functionalization of proline and pyrrolidine derivatives,[60] we probed the enantioselectivity in the capture of α-amino radical **43** by nickel(II) complexes **44** and **47** bearing chiral pyrox and bis(imidazoline) ligands, respectively. Both **44** and **47** are diamagnetic complexes, which fits the general profile of square planar nickel(II)-aryl complexes. Upon irradiation, DHP derivative **42** underwent bond homolysis to eject radical **43**. In the presence of **44**, the radical proceeded to generate cross-coupling product (*S*)-**46** in 35% enantiomeric excess (ee). In contrast, complex **47** trapped **43** to furnish the opposite enantiomer of (*R*)-**46** in −94% ee.

The low yields were associated with inefficient radical generation and decomposition side pathways of the nickel complexes. It is conceivable that radical **43** was trapped by **44** and **47** to afford Ni(III) intermediates **45** and **48**, respectively. The C1 symmetric pyrox ligand and the C2 symmetric bis(imidazoline) ligands favor two different enantiomers. The high ee delivered by bis(imidazoline) is corroborated by the optimized catalytic conditions.[60] Although the reversibility of radical trapping at **44** and **47** is uncertain at this point, these results highlight the impact of ligand frameworks on enantioselectivity.

Conclusion

In summary, we have established the structure-activity relationship of radical capture at catalytically relevant nickel(II) complexes supported on bpy, phen, pyrox, and pybox ligands. The significant steric effect of the actor ligand and the observation of homo-coupling products, along with the EPR characterization of a resulting nickel(III) intermediate, provide experimental evidence for an inner-sphere mechanism for radical capture and C–C bond formation. Radical addition to nickel-aryl complexes led to fast and clean formation of the cross-coupling product, whereas nickel-alkyl complexes proved inefficient at mediating C(sp^3)–C(sp^3) bond formation. This remarkable difference in reactivity between nickel-aryl and nickel-alkyl complexes with the same ancillary ligand was attributed to different rate-determining steps and highlights challenges in cross-coupling reactions to form C(sp^3)–C(sp^3) bonds. This result has important implications in envisioning the scope of catalytic reactions involving radical capture by nickel. Kinetic characterization reveals higher activation energy (7.0–7.5 kcal/mol for primary radicals and 8.7–9.2 kcal/mol for secondary radicals) than previous DFT results, which resolves inconsistencies among different computational studies and suggests that radical trapping could be slower than reductive elimination. Primary radicals are trapped faster than secondary radicals by over an order of magnitude. Finally, stoichiometric studies demonstrate that

the radical capture step can confer diastereoselectivity and enantioselectivity in mediating cross-coupling reactions.

EXPERIMENTAL PROCEDURES

Lead contact

Information regarding experimental procedures and requests for resources, data, and reagents should be directed to the lead contact, Tianning Diao (diao@nyu.edu).

Materials availability

Full experimental details, including complex synthesis, spectroscopic measurements, rate data, and ^{1}H NMR, ^{13}C NMR, mass spectrometry, and EPR data, are available in the supplemental information for all unique compounds. There are restrictions to the availability of all reagents and products because of limitations on our capacity to store compounds. Raw data are available from the lead contact upon request.

Data and code availability

All data supporting this study are available in the manuscript and supplemental information. Additional information is available from the lead contact upon request.

SUPPLEMENTAL INFORMATION

Supplemental information can be found online at https://doi.org/10.1016/j.chempr.2023.02.010.

ACKNOWLEDGMENTS

This work was supported by the National Institutes of Health (R01GM127778). Q.L. thanks the Margaret and Herman Sokol Fellowship and the GSAS Dean's Dissertation Fellowship. T.D. thanks the Camille and Henry Dreyfus Foundation (TC-19-019) for providing fellowships to partially support this work.

AUTHORS CONTRIBUTIONS

Q.L. and T.D. conceived the project. Q.L. and E.S. conducted the experiments. Q.L., E.S., and T.D. analyzed and interpreted the results. T.D. wrote the manuscript.

DECLARATION OF INTERESTS

The authors declare no competing interests.

Received: October 26, 2022
Revised: December 28, 2022
Accepted: February 10, 2023
Published: March 13, 2023

REFERENCES

1. Tasker, S.Z., Standley, E.A., and Jamison, T.F. (2014). Recent advances in homogeneous nickel catalysis. Nature *509*, 299–309.
2. Choi, J., and Fu, G.C. (2017). Transition metal–catalyzed alkyl-alkyl bond formation: another dimension in cross-coupling chemistry. Science *356*, eaaf7230.
3. Fu, G.C. (2017). Transition-metal catalysis of nucleophilic substitution reactions: a radical alternative to SN1 and SN2 processes. ACS Cent. Sci. *3*, 692–700.
4. Diccianni, J.B., and Diao, T. (2019). Mechanisms of nickel-catalyzed cross-coupling reactions. J. Trends Chem. *1*, 830–844.
5. Chan, A.Y., Perry, I.B., Bissonnette, N.B., Buksh, B.F., Edwards, G.A., Frye, L.I., Garry, O.L., Lavagnino, M.N., Li, B.X., Liang, Y., et al. (2022). Metallaphotoredox: the merger of photoredox and transition metal catalysis. Chem. Rev. *122*, 1485–1542.
6. Zhu, S., Zhao, X., Li, H., and Chu, L. (2021). Catalytic three-component dicarbofunctionalization reactions involving radical capture by nickel. Chem. Soc. Rev. *50*, 10836–10856.
7. Schley, N.D., and Fu, G.C. (2014). Nickel-catalyzed Negishi arylations of propargylic

bromides: a mechanistic investigation. J. Am. Chem. Soc. *136*, 16588–16593.

8. Lin, Q., Fu, Y., Liu, P., and Diao, T. (2021). Monovalent nickel-mediated radical formation: a concerted halogen-atom dissociation pathway determined by electroanalytical studies. J. Am. Chem. Soc. *143*, 14196–14206.

9. Crespi, S., and Fagnoni, M. (2020). Generation of alkyl radicals: from the tyranny of tin to the photon democracy. Chem. Rev. *120*, 9790–9833.

10. Kvasovs, N., and Gevorgyan, V. (2021). Contemporary methods for generation of aryl radicals. Chem. Soc. Rev. *50*, 2244–2259.

11. Sumida, Y., and Ohmiya, H. (2021). Direct excitation strategy for radical generation in organic synthesis. Chem. Soc. Rev. *50*, 6320–6332.

12. Zheng, B., Tang, F., Luo, J., Schultz, J.W., Rath, N.P., and Mirica, L.M. (2014). Organometallic nickel(III) complexes relevant to cross-coupling and carbon–heteroatom bond formation reactions. J. Am. Chem. Soc. *136*, 6499–6504.

13. Bour, J.R., Camasso, N.M., Meucci, E.A., Kampf, J.W., Canty, A.J., and Sanford, M.S. (2016). Carbon-carbon bond-forming reductive elimination from isolated nickel(III) complexes. J. Am. Chem. Soc. *138*, 16105–16111.

14. Lin, Q., and Diao, T. (2019). Mechanism of Ni-catalyzed reductive 1,2-dicarbofunctionalization of alkenes. J. Am. Chem. Soc. *141*, 17937–17948.

15. Lucas, E.L., and Jarvo, E.R. (2017). Stereospecific and stereoconvergent cross-couplings between alkyl electrophiles. Nat. Rev. Chem. *1*.

16. Cherney, A.H., Kadunce, N.T., and Reisman, S.E. (2015). Enantioselective and enantiospecific transition-metal-catalyzed cross-coupling reactions of organometallic reagents to construct C–C bonds. Chem. Rev. *115*, 9587–9652.

17. Bakac, A., and Espenson, J.H. (1986). Kinetics and mechanism of the alkylnickel formation in one-electron reductions of alkyl-halides and hydroperoxides by a macrocyclic nickel(I) complex. J. Am. Chem. Soc. *108*, 713–719.

18. Vorobyev, D.Y., Plyusnin, V.F., Ivanov, Y.V., Grivin, V.P., Larionov, S.V., and Lemmetyinen, H. (2002). Photochromic reactions of reversible coordination of perfluorothionaphthyl radical with flat Ni(II) dithiolate complexes. J. Photochem. Photobiol. A *149*, 101–109.

19. Bakhoda, A.G., Wiese, S., Greene, C., Figula, B.C., Bertke, J.A., and Warren, T.H. (2020). Radical capture at nickel(II) complexes: C–C, C–N, and C–O bond formation. Organometallics *39*, 1710–1718.

20. Shin, J., Gwon, S., Kim, S., Lee, J., and Park, K. (2020). Correlation between the C–C cross-coupling activity and C-to-Ni charge transfer transition of high-valent Ni complexes. J. Am. Chem. Soc. *142*, 4173–4183.

21. Bour, J.R., Ferguson, D.M., McClain, E.J., Kampf, J.W., and Sanford, M.S. (2019). Connecting organometallic Ni(III) and Ni(IV): reactions of carbon-centered radicals with high-valent organonickel complexes. J. Am. Chem. Soc. *141*, 8914–8920.

22. Gutierrez, O., Tellis, J.C., Primer, D.N., Molander, G.A., and Kozlowski, M.C. (2015). Nickel-catalyzed cross-coupling of photoredox-generated radicals: uncovering a general manifold for stereoconvergence in nickel-catalyzed cross-couplings. J. Am. Chem. Soc. *137*, 4896–4899.

23. Shu, W., García-Domínguez, A., Quirós, M.T., Mondal, R., Cárdenas, D.J., and Nevado, C. (2019). Ni-catalyzed reductive dicarbofunctionalization of nonactivated alkenes: scope and mechanistic insights. J. Am. Chem. Soc. *141*, 13812–13821.

24. Yuan, M., Song, Z., Badir, S.O., Molander, G.A., and Gutierrez, O. (2020). On the nature of C(sp^3)–C(sp^2) bond formation in nickel-catalyzed tertiary radical cross-couplings: a case study of Ni/photoredox catalytic cross-coupling of alkyl radicals and aryl halides. J. Am. Chem. Soc. *142*, 7225–7234.

25. Matsui, J.K., Gutiérrez-Bonet, Á., Rotella, M., Alam, R., Gutierrez, O., and Molander, G.A. (2018). Photoredox/nickel-catalyzed single-electron Tsuji-Trost reaction: development and mechanistic insights. Angew. Chem. Int. Ed. *57*, 15847–15851.

26. Campbell, M.W., Yuan, M., Polites, V.C., Gutierrez, O., and Molander, G.A. (2021). Photochemical C–H activation enables nickel-catalyzed olefin dicarbofunctionalization. J. Am. Chem. Soc. *143*, 3901–3910.

27. Kolahdouzan, K., Khalaf, R., Grandner, J.M., Chen, Y., Terrett, J.A., and Huestis, M.P. (2020). Dual photoredox/nickel-catalyzed conversion of aryl halides to aryl aminooxetanes: computational evidence for a substrate-dependent switch in mechanism. ACS Catal. *10*, 405–411.

28. Lau, S.H., Borden, M.A., Steiman, T.J., Wang, L.S., Parasram, M., and Doyle, A.G. (2021). Ni/photoredox-catalyzed enantioselective cross-electrophile coupling of styrene oxides with aryl iodides. J. Am. Chem. Soc. *143*, 15873–15881.

29. Yin, H., and Fu, G.C. (2019). Mechanistic investigation of enantioconvergent Kumada reactions of racemic α-bromoketones catalyzed by a nickel/bis(oxazoline) complex. J. Am. Chem. Soc. *141*, 15433–15440.

30. Guo, L., Yuan, M., Zhang, Y., Wang, F., Zhu, S., Gutierrez, O., and Chu, L. (2020). General method for enantioselective three-component carboarylation of alkenes enabled by visible-light dual photoredox/nickel catalysis. J. Am. Chem. Soc. *142*, 20390–20399.

31. Xu, J., Yang, Y., Zhao, X., Liu, C., and Zhang, D. (2021). DFT mechanistic study of IrIII/NiII-metallaphotoredox-catalyzed difluoromethylation of aryl bromides. Inorg. Chem. *60*, 8682–8691.

32. Yuan, M., and Gutierrez, O. (2022). Mechanisms, challenges, and opportunities of dual Ni/photoredox-catalyzed C(sp^2)–C(sp^3) cross-couplings. Wiley Interdiscip. Rev. Comput. Mol. Sci. *12*, e1573.

33. Buzzetti, L., Prieto, A., Roy, S.R., and Melchiorre, P. (2017). Radical-based C–C bond-forming processes enabled by the photoexcitation of 4-alkyl-1,4-dihydropyridines. Angew. Chem. Int. Ed. *56*, 15039–15043.

34. Shields, B.J., Kudisch, B., Scholes, G.D., and Doyle, A.G. (2018). Long-lived charge-transfer states of nickel(II) aryl halide complexes facilitate bimolecular photoinduced electron transfer. J. Am. Chem. Soc. *140*, 3035–3039.

35. Efforts to synthesize phen and (^{tBu}bpy)Ni-methyl and ethyl complexes were complicated by their instability. The neosilyl group can stabilize the nickel complex by β-effect of the silicon, which is not believed to make a drastic difference in the reactivity.

36. Yamano, M.M., Kelleghan, A.V., Shao, Q., Giroud, M., Simmons, B.J., Li, B., Chen, S., Houk, K.N., and Garg, N.K. (2020). Intercepting fleeting cyclic allenes with asymmetric nickel catalysis. Nature *586*, 242–247.

37. Complex **6** was unstable and exhibited trace paramagnetic impurity in the EPR spectrum before irradiation and was thus excluded from the EPR study.

38. Hagen, W.R. (2009). Biomolecular EPR spectroscopy. In Biomolecular EPR Spectroscopy (CRC Press), p. 65.

39. Roessler, M.M., and Salvadori, E. (2018). Principles and applications of EPR spectroscopy in the chemical sciences. Chem. Soc. Rev. *47*, 2534–2553.

40. Que, L., Jr. (2000). Physical methods in bioinorganic chemistry spectroscopy and magnetism. In Physical Methods in Bioinorganic Chemistry Spectroscopy and Magnetism (University Science Books), p. 123.

41. Abe, M. (2013). Diradicals. Chem. Rev. *113*, 7011–7088.

42. Le Vaillant, F., Reijerse, E.J., Leutzsch, M., and Cornella, J. (2020). Dialkyl ether formation at high-valent nickel. J. Am. Chem. Soc. *142*, 19540–19550.

43. Xu, H., Diccianni, J.B., Katigbak, J., Hu, C., Zhang, Y., and Diao, T. (2016). Bimetallic C–C bond-forming reductive elimination from nickel. J. Am. Chem. Soc. *138*, 4779–4786.

44. Newcomb, M. (1993). Competition methods and scales for alkyl radical reaction kinetics. Tetrahedron *49*, 1151–1176.

45. Newcomb, M., Filipkowski, M.A., and Johnson, C.C. (1995). α-ethoxycarbonyl and α-methoxy substituted radical clocks. Tetrahedron Lett. *36*, 3643–3646.

46. Newcomb, M., Horner, J.H., Filipkowski, M.A., Ha, C., and Park, S.-U. (1995). Absolute rate constants for reactions of alpha-carbethoxy and alpha-cyano radicals. J. Am. Chem. Soc. *117*, 3674–3684.

47. Kuang, Y., Wang, X., Anthony, D., and Diao, T. (2018). Ni-catalyzed two-component reductive dicarbofunctionalization of alkenes via radical cyclization. Chem. Commun. *54*, 2558–2561.

48. Cohen, A.J., Mori-Sánchez, P., and Yang, W. (2008). Insights into current limitations of density functional theory. Science *321*, 792–794.

49. Hartwig, J.F. (2007). Electronic effects on reductive elimination to form carbon−carbon and carbon−heteroatom bonds from palladium(II) complexes. Inorg. Chem. *46*, 1936–1947.

50. Bowes, E.G., Pal, S., and Love, J.A. (2015). Exclusive Csp^3–Csp^3 vs Csp^2–Csp^3 reductive elimination from PtIV governed by ligand constraints. J. Am. Chem. Soc. *137*, 16004–16007.

51. Yamamoto, T., Yamamoto, A., and Ikeda, S. (1971). Organo (dipyridyl) nickel complexes. I. Stability and activation of the alkyl-nickel bonds of dialkyl (dipyridyl) nickel by coordination with various substituted olefins. J. Am. Chem. Soc. *93*, 3350–3359.

52. Low, J.J., and Goddard, W.A. (1984). Reductive coupling of hydrogen-hydrogen, hydrogen-carbon, and carbon-carbon bonds from palladium complexes. J. Am. Chem. Soc. *106*, 8321–8322.

53. Qin, T., Cornella, J., Li, C., Malins, L.R., Edwards, J.T., Kawamura, S., Maxwell, B.D., Eastgate, M.D., and Baran, P.S. (2016). A general alkyl-alkyl cross-coupling enabled by redox-active esters and alkylzinc reagents. Science *352*, 801–805.

54. Smith, R.T., Zhang, X., Rincón, J.A., Agejas, J., Mateos, C., Barberis, M., García-Cerrada, S., de Frutos, O., and MacMillan, D.W.C. (2018). Metallaphotoredox-catalyzed cross-electrophile Csp^3–Csp^3 coupling of aliphatic bromides. J. Am. Chem. Soc. *140*, 17433–17438.

55. Komeyama, K., Michiyuki, T., and Osaka, I. (2019). Nickel/cobalt-catalyzed $C(sp^3)$–$C(sp^3)$ cross-coupling of alkyl halides with alkyl tosylates. ACS Catal. *9*, 9285–9291.

56. Schultz, J.W., Fuchigami, K., Zheng, B., Rath, N.P., and Mirica, L.M. (2016). Isolated organometallic nickel(III) and nickel(IV) complexes relevant to carbon–carbon bond formation reactions. J. Am. Chem. Soc. *138*, 12928–12934.

57. Dumoulin, A., Matsui, J.K., Gutiérrez-Bonet, Á., and Molander, G.A. (2018). Synthesis of non-classical arylated C-saccharides through nickel/photoredox dual catalysis. Angew. Chem. Int. Ed. *57*, 6614–6618.

58. Wei, Y., Ben-Zvi, B., and Diao, T. (2021). Diastereoselective synthesis of aryl C-glycosides from glycosyl esters via C−O bond homolysis. Angew. Chem. Int. Ed. *60*, 9433–9438.

59. Wei, Y., Lam, J., and Diao, T. (2021). Synthesis of C-acyl furanosides via the cross-coupling of glycosyl esters with carboxylic acids. Chem. Sci. *12*, 11414–11419.

60. Shu, X., Zhong, D., Lin, Y., Qin, X., and Huo, H. (2022). Modular access to chiral α-(hetero)aryl amines via Ni/photoredox-catalyzed enantioselective cross-coupling. J. Am. Chem. Soc. *144*, 8797–8806.